Available online at www.sciencedirect.com
SCIENCE DIRECT®
Pergamon
Acta Materialia 51 (2003) 1167–1179
Acta MATERIALIA
www.actamat-journals.com

# Difference in compressive and tensile fracture mechanisms of $Zr_{59}Cu_{20}Al_{10}Ni_8Ti_3$ bulk metallic glass

Z.F. Zhang *, J. Eckert, L. Schultz

*IFW Dresden, Institute for Metallic Materials, P.O. Box 270016, D-01171, Dresden, Germany*

Received 12 August 2002; accepted 12 October 2002

**Abstract**

The compressive and tensile deformation, as well as the fracture behavior of a $Zr_{59}Cu_{20}Al_{10}Ni_8Ti_3$ bulk metallic glass were investigated. It was found that under compressive loading, the metallic glass displays some plasticity before fracture. The fracture is mainly localized on one major shear band and the compressive fracture angle, $\theta_C$, between the stress axis and the fracture plane is 43°. Under tensile loading, the material always displays brittle fracture without yielding. The tensile fracture stress, $\sigma_F^T$, is about 1.58 GPa, which is lower than the compressive fracture stress, $\sigma_F^C$( = 1.69 GPa). The tensile fracture angle, $\theta_T$, between the stress axis and the fracture plane is equal to 54°. Therefore, both $\theta_C$ and $\theta_T$ deviate from the maximum shear stress plane (45°), indicating that the fracture behavior of the metallic glass under compressive and tensile load does not follow the von Mises criterion. Scanning electron microscope observations reveal that the compressive fracture surfaces of the metallic glass mainly consist of a vein-like structure. A combined feature of veins and some radiate cores was observed on the tensile fracture surfaces. Based on these results, the fracture mechanisms of metallic glass are discussed by taking the effect of normal stress on the fracture process into account. It is proposed that tensile fracture first originates from the radiate cores induced by the normal stress, then propagates mainly driven by shear stress, leading to the formation of the combined fracture feature. In contrast, the compressive fracture of metallic glass is mainly controlled by the shear stress. It is suggested that the deviation of $\theta_C$ and $\theta_T$ from 45° can be attributed to a combined effect of the normal and shear stresses on the fracture plane.


*Keywords:* Metallic glass; Deformation and fracture; Shear bands; Fracture angle

## 1. Introduction

Bulk metallic glasses (BMGs) have many potential applications due to their unique properties, for example, superior strength and high hardness, excellent corrosion resistance and high wear resistance [1,2]. However, the high strength of BMGs is often accompanied by remarkably little plastic deformation and their deformation and fracture mechanisms are quite different from crystalline materials [3–12]. As is well known, there are several plastic deformation modes, such as slipping, shearing, kinking and twining, in crystalline materials [13], and yielding of most single crystals

* Corresponding author. On leave from Shenyang National Laboratory for Materials Sciences, Institute of Metal Research, Chinese Academy of Science, Shenyang 110016, P.R. China. Tel.: +49-351-465-9766; fax: +49-351-465-9541.
*E-mail address:* z.f.zhang@ifw-dresden.de (Z.F. Zhang).

1359-6454/03/$30.00 
doi:10.1016/S1359-6454(02)00521-9

follows Schmid's law. In general, single crystals often slide along the slip system with the largest Schmid factor. As a result, the yield stress and the angle, $\theta$, between the slip plane and the stress axis can be calculated from the orientation of the single crystal.

In the past three decades, the deformation and fracture behavior of metallic glasses was widely investigated [3–12]. In general, the plastic deformation of metallic glasses is localized in the narrow shear bands, followed by the rapid propagation of these shear bands and sudden fracture. Meanwhile, the following deformation and fracture behavior of metallic glasses was often observed. (1) Under compressive load, metallic glasses deform and fracture along localized shear bands and the fracture angle, $\theta_C$, between the compressive axis and the shear plane is, in general, smaller than 45° (about 42°) [14–17]. (2) Under tensile load, however, it is found that the tensile fracture angle, $\theta_T$, between the tensile axis and the fracture plane is larger than 45°. In most cases, $\theta_T$ is in the range 50–65° with an average value of 56° [15–24]. This indicates that the deformation and fracture of metallic glasses will not occur along the maximum shear stress plane irrespective of whether they are under compressive or tensile load. Donovan [9] has proposed a yield criterion for $Pd_{40}Ni_{40}P_{20}$ metallic glass under compressive load. He found that the yield behavior of the glass follows a Mohr–Coulomb criterion rather than the von Mises criterion. Since the difference in the fracture angles $\theta_C$ and $\theta_T$ is quite large, however, there is no reasonable explanation for this phenomenon, which should be of special importance for a better understanding of the deformation mechanisms of metallic glasses. In the present work, we attempt to further reveal the basic deformation and fracture mechanisms through compressive and tensile tests of a $Zr_{59}Cu_{20}Al_{10}Ni_8Ti_3$ BMG.

## 2. Experimental procedure

Master ingots with composition $Zr_{59}Cu_{20}Al_{10}Ni_8Ti_3$ were prepared by arc-melting elemental Zr, Cu, Al, Ni and Ti with a purity of 99.9% or better in a Ti-gettered argon atmosphere. For reaching homogeneity, the master alloy ingots were remelted several times and were subsequently cast into copper molds with different dimensions, i.e. 40 mm × 30 mm × 1.8 mm for tensile test specimens and 3 mm in diameter and 50 mm in length for the samples used for compressive tests. The amorphous structure of the samples was checked by standard X-Ray diffraction (XRD) (Philips PW1050 diffractometer using Co-K$\alpha$ radiation). As shown in Fig. 1, the two kinds of samples for the compressive and tensile tests show only broad diffraction maxima and no peaks of crystalline phases can be seen, revealing the amorphous structure of the samples. For compressive tests, the 50-mm long rods were cut into specimens of 6 mm in length and 3 mm in diameter. Tensile specimens with a total length of 40 mm were machined from the plates and were polished to produce a mirror surface. The final gauge dimension of the specimens was 6 mm × 3 mm × 1.5 mm. The compression and the tensile tests were conducted at different strain rates with an Instron 4466 testing machine at room temperature. After fracture, all the specimens were investigated by a JEOL JSM6400 scanning electron microscope (SEM) and by an optical microscope (OM) to reveal the fracture surface morphology and the fracture features.

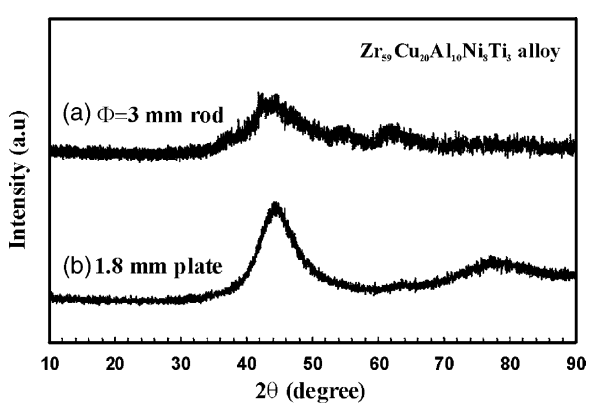


Fig. 1. XRD patterns of $Zr_{59}Cu_{20}Al_{10}Ni_8Ti_3$ metallic glass for (a) compressive and (b) tensile tests.

## 3. Experimental results

### 3.1. Stress–strain curves

Fig. 2(a) shows the compressive stress–strain curves of the metallic glass specimens at strain rates of $4.5 \times 10^{-5}$ $s^{-1}$ and $4.5 \times 10^{-3}$ $s^{-1}$. It can be seen that the metallic glassy samples display an initial elastic deformation behavior with an elastic strain of 1.5%, then begin to yield at about 1.45 GPa, followed by some strain hardening before fracture. The compressive plastic strains for the two specimens are 0.52 and 0.60%, respectively. Obviously, the metallic glass can deform with certain plasticity under compressive load. The compressive fracture stress, $\sigma_F^C$, reaches $1.69 \pm 0.02$ GPa, the measured Young modulus is equal to $91.1 \pm 1.8$ GPa for the two specimens deformed at the strain rates of $4.5 \times 10^{-5}$ $s^{-1}$ and $4.5 \times 10^{-3}$ $s^{-1}$. These results indicate that the fracture stress, the elastic and plastic strains and Young's modulus are not significantly affected by the applied strain rates under compressive loading. The present results are consistent with other data for Zr–Cu–Al–Ni–Ti metallic glasses [25–27].

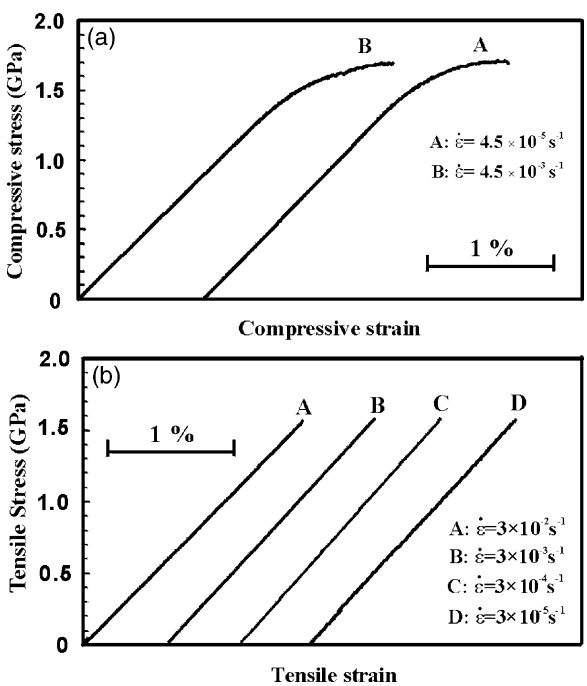


Fig. 2. Stress–strain curves of $Zr_{59}Cu_{20}Al_{10}Ni_8Ti_3$ metallic glassy specimens for different strain rates under (a) compressive loading and (b) tensile loading.

Fig. 2(b) gives the tensile stress–strain curves of the metallic glassy specimens deformed in the strain rate range $3 \times 10^{-5}$ to $3 \times 10^{-2}$ $s^{-1}$. All the specimens display only an elastic deformation behavior and catastrophic fracture without yielding, which is different from the compressive tests. The fracture stress, $\sigma_F^T$, of the four specimens nearly maintains a constant value of 1.56–1.60 GPa, independent of the applied strain rates. The total tensile strain before failure is about 1.7%, the average fracture stress, $\sigma_F^T$, is $1.58 \pm 0.02$ GPa, which is silightly lower than the compressive fracture stress, $\sigma_F^C$ ($1.69 \pm 0.02$ GPa).

From the compressive and tensile tests, it can be deduced that, as expected, the fracture stress is independent of the strain rate, which was also observed for other metallic glasses [24]. Another difference in the deformation mechanisms of the two different testing modes is the occurrence of plastic deformation and a relatively high fracture stress under compression even though the glassy specimens have the same composition. A similar phenomenon was widely observed for a variety of most metallic glasses [17,20]. The difference in the deformation mechanisms should be attributed to the effect of loading modes and will be further discussed in the following sections.

### 3.2. Fracture surface observations

#### 3.2.1. Compressive fracture feature

SEM observations show that the fracture under compression always occurs in a shear mode, as seen in Fig. 3(a), the compressive fracture surface has a large angle $\theta_C$ with the stress axis and can be measured as marked in the figure. It is found that $\theta_C$ is equal to 43° for the present specimens. As one can see in Fig. 3(b), the fracture surface is relatively flat and displays a typical shear fracture feature, such as it has been widely observed for many other metallic glass specimens [14–17]. In most metallic glasses, it was found that the compressive fracture angle, $\theta_C$, deviates from 45°. For comparison, some measured results for $\theta_C$ are listed in Table 1. It can be seen that, in general,

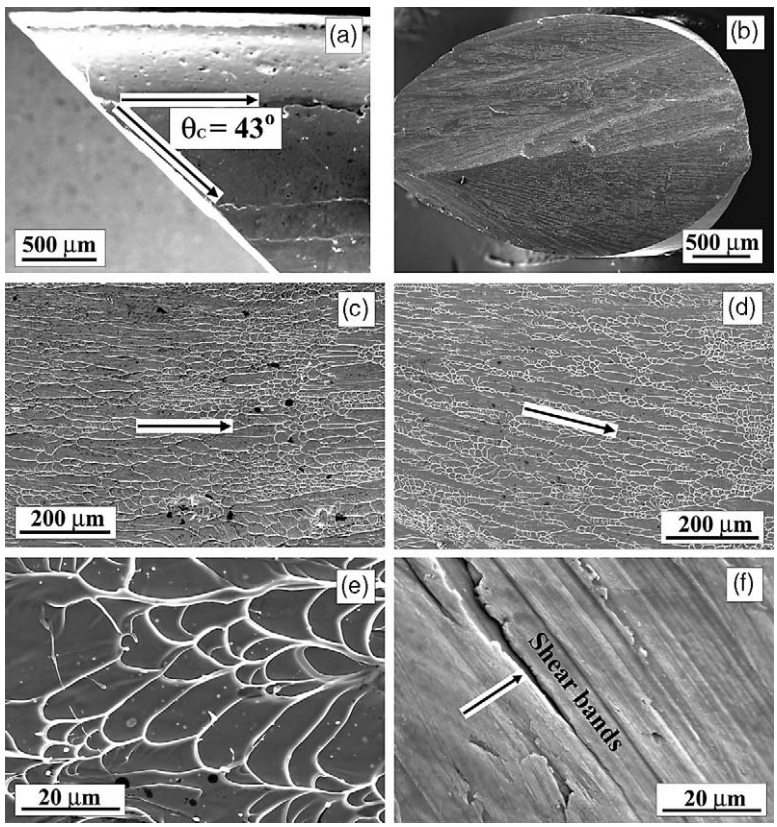


Fig. 3. SEM micrographs revealing the compressive fracture feature of $Zr_{59}Cu_{20}Al_{10}Ni_8Ti_3$ metallic glass. (a) Shear fracture of the compressive specimen; (b)–(e) compressive fracture surface at different magnification; (f) shear bands on the specimen surface.

Table 1
Comparison of the compressive fracture angle, $\theta_C$, for different metallic glasses

| Investigators | Metallic glasses | Fracture angle ($\theta_C$) |
|---|---|---|
| Donovan [14] | $Pd_{40}Ni_{40}P_{20}$ | $\theta_C = 41.9 \pm 1.2°$ |
| Lowhaphandu et al. [15] | $Zr_{62}Ti_{10}Ni_{10}Cu_{14.5}Be_{3.5}$ | $\theta_C = 41.6 \pm 2.1°$ |
| Wright et al. [16] | $Zr_{40}Ti_{14}Ni_{10}Cu_{12}Be_{24}$ | $\theta_C = 42°$ |
| He et al. [17] | $Zr_{52.5}Ni_{14.6}Al_{10}Cu_{17.9}Ti_5$ | $\theta_C = 40–45°$ |
| Present results | $Zr_{59}Cu_{20}Al_{10}Ni_8Ti_3$ | $\theta_C = 43°$ |

$\theta_C$ is approximately equal to 42–43°, i.e. smaller than 45°. This indicates that the compressive fracture of metallic glasses does not occur along the plane of the maximum shear stress and accordingly, does not follow the von Mises criterion [9].

Further observations show that the typical feature of the fracture surfaces is a vein-like structure, as shown in Fig. 3(c) and (d). This vein-like structure often spreads over the whole fracture surface and extends along a uniform direction, as marked by arrows in the two figures. It is noted that the uniform arrangement of the veins exactly corresponds to the propagation direction of the shear band, which is confirmed by Fig. 3(b). The vein-like structure was attributed to local melting within the main shear band induced by the high elastic

energy in instantaneous fracture [16,20]. Due to the melting of metallic glass within the main shear band, the molten metallic glass easily flows and appears in a vein-like structure feature, as clearly shown in Fig. 3(e). For all metallic glasses, their compressive fracture surfaces nearly show the same features, i.e. a vein-like structure [9,20,22,25–27]. These veins on the fractography clearly demonstrate a pure shear fracture process of the different metallic glasses.

When the investigations are focused on the specimen surfaces, it is noted that there are many localized shear bands near the fracture plane, as shown in Fig. 3(f). The shear bands have a relatively high density and are basically parallel to the fracture plane. The activation of the shear bands should be a direct evidence for the compressive plasticity of the metallic glass. However, the shear bands did not propagate over the whole specimen surface. This indicates that the plastic deformation only took place at a local region near the fracture surface. Within these shear bands, occasionally, one or two cracks can be seen, as indicated by the arrow in Fig. 3(f).

*3.2.2. Tensile fracture feature*

OM and SEM observations show that the tensile specimens also fractured in a shear mode, as shown in Fig. 4(a). The formation and propagation of one major shear band dominates the fracture process. The fracture surface is very smooth and a vein-like morphology is visible (Fig. 4(b)). Therefore, the tensile fracture angle, $\theta_T$, between the tensile axis and the fracture plane can be readily measured on the surface of the specimen, as marked in Fig. 4(a). It is found that the tensile fracture angles, $\theta_T$, of the present specimens are equal to 54°, which is significantly different from 45°. The present result is consistent with previous observations for other metallic glasses under tensile deformation [5,15–24]. For comparison, all the available results for $\theta_T$ are listed in Table 2. Apparently, $\theta_T$ is, in general, in the range 50–65° for different metallic glasses, which obviously deviates from the angle of the maximum shear stress plane (45°). Therefore, it can be concluded that the tensile deformation behavior of metallic glasses should also not follow the von Mises criterion [9].

Further investigations reveal that the morphology on the tensile fracture surface is quite peculiar in comparison with that on the compressive fracture surfaces. On the tensile fracture surface, besides the vein-like structure, there are many round cores with different diameters on the whole surface, as shown in Fig. 4(b)–(d). In previous observations, there have been some similar features on tensile fracture surfaces. The features reported are comparable to those in the literature [5] (Figs. 8 and 13), [24] (Fig. 5), [28] (Fig. 8) and [29] (Fig. 5), respectively. However, these cores were never mentioned in detail before and were not considered for respondence to the fracture mechanisms of metallic glasses subjected to tensile deformation. All the micrographs demonstrate that the cores coexist with the vein-like structure and the veins radiate from these cores and propagate towards outside, as clearly shown in Fig. 4(e). In the region of the cores, the fracture seems to take place in a normal fracture mode, rather than a pure shear mode. From this morphology, it is suggested that the fracture of metallic glasses should first originate from these cores induced by normal tension stress on the plane, then catastrophically propagate towards outside of the cores in a shear mode driven by the shear stress. As a result, the tensile fracture surface of metallic glasses consists of a combined feature of cores and veins, which is quite different from the compressive fracture surface. Therefore, the above fracture morphology should reflect the difference in the fracture mechanisms of metallic glasses under compressive and tensile loading and will be further discussed in Section 4. On the specimen surface, it is found that there are also some shear bands, as shown in Fig. 4(f). However, in comparison with the dense shear band array in Fig. 3(f), there are only 3–4 shear bands on the specimen surface. This indicates that the shear bands induced by tensile loading are rather few and consequently, do not contribute much to the overall tensile plasticity, as shown in the curves of Fig. 2(b).

## 4. Discussion

From the above observations, it can be concluded that the fracture processes of the metallic

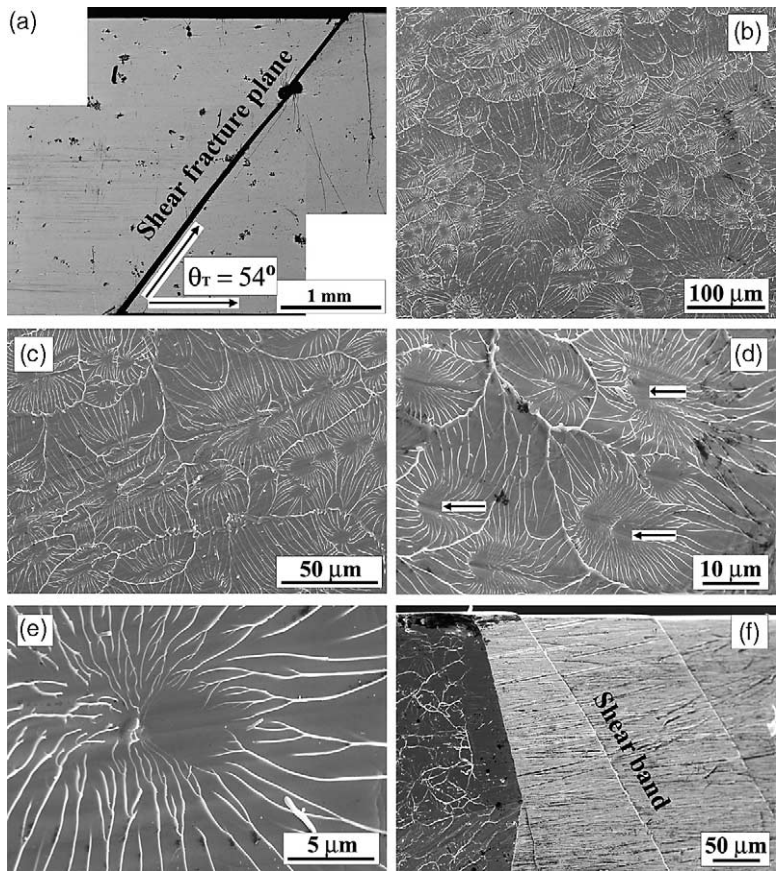


Fig. 4. SEM micrographs revealing the tensile fracture feature of $Zr_{59}Cu_{20}Al_{10}Ni_8Ti_3$ metallic glass. (a) Shear fracture of the tensile specimen; (b)–(e) tensile fracture surface at different magnification; (f) shear band on the specimen surface.

Table 2
Comparison of the tensile fracture angle, $\theta_T$, for different metallic glasses

| Investigators | Metallic glasses | Fracture angle ($\theta_T$) |
|---|---|---|
| Pampillo [5] | $Pd_{80}Si_{20}$ | $\theta_T = 54.7°$ |
| Lowhaphandu et al. [15] | $Zr_{62}Ti_{10}Ni_{10}Cu_{14.5}Be_{3.5}$ | $\theta_T = 57 \pm 3.7°$ |
| Wright et al. [16] | $Zr_{40}Ti_{14}Ni_{10}Cu_{12}Be_{24}$ | $\theta_T = 56°$ |
| He et al. [17] | $Zr_{52.5}Ni_{14.6}Al_{10}Cu_{17.9}Ti_5$ | $\theta_T = 55–65°$ |
| Takayama [18] | $Pd_{77.5}Cu_6Si_{16.5}$ | $\theta_T = 51°$ |
| Megusar et al. [19] | $Pd_{80}Si_{20}$ | $\theta_T = 50°$ |
| Liu et al. [20] | $Zr_{52.5}Ni_{14.6}Al_{10}Cu_{17.9}Ti_5$ | $\theta_T = 53–60°$ |
| Fan and Inoue [21] | $Zr_{60}Al_{10}Cu_{20}Pd_{20}$ | $\theta_T = 50°$ |
| Inoue et al. [22] | $Zr_{65}Ni_{10}Al_{7.5}Cu_{7.5}Pd_{10}$ | $\theta_T = 50°$ |
| Inoue et al. [23] | $Cu_{60}Zr_{30}Ti_{10}$ | $\theta_T = 54°$ |
| Mukai et al. [24] | $Pd_{40}Ni_{40}P_{20}$ | $\theta_T = 56°$ |
| Present results | $Zr_{59}Cu_{20}Al_{10}Ni_8Ti_3$ | $\theta_T = 54°$ |

glass under compressive and tensile loading are significantly different. For comparison, two typical fractography morphologies induced by compressive and tensile fracture are shown in Fig. 5(a) and (b) again. First, all the above observations in Fig. 3(b)–(e) and Fig. 5(a) demonstrate that the compressive fracture surfaces only exhibit a vein-like structure with a rather uniform arrangement. This indicates that the compressive fracture should occur in a pure shear mode, along the direction indicated by the arrow in Fig. 5(a). However, for the tensile fracture surface, there are two types of features, i.e. some cores and the veins (Fig. 5(b)). It is apparent that the veins should originate from the cores and propagate radially towards outside. Therefore, the tensile fracture should not occur in a pure shear mode, i.e. is different from that under compression. This suggests that the fracture processes of metallic glass are strongly affected by the loading modes. The main reason for this can be attributed to the effect of the normal stress. According to the observations above, the compressive fracture processes of the metallic glass can be illustrated as in Fig. 6(a) and (b). Under compressive loading, the normal stress $\sigma_\theta^C$ always exerts on the fracture plane in a compressive mode. Consequently, the fracture process of metallic glass should be mainly controlled by the shear stress $\tau_\theta^C$, as illustrated in Fig. 6(b). The uniform arrangement of the veins on the fracture surface provides a direct evidence for this assumption. However, the tensile fracture processes of metallic glass should be different from the compressive fracture because the cores always appear on the whole fracture surface. Fig. 7(a) demonstrates the initial stage of nucleation of the cores induced by the normal tension stress, $\sigma_\theta^T$. Once these cores are formed, they will propagate rapidly towards the outside mainly driven by the shear stress $\tau_\theta^T$ and connect to each other, as illustrated in Fig. 7(b). Finally, the rapid propagation of the cores results in a catastrophic fracture, and forms a combined feature of the cores and the veins, as illustrated in Fig. 7(c). This is well consistent with the observations in Fig. 4(b)–(e).

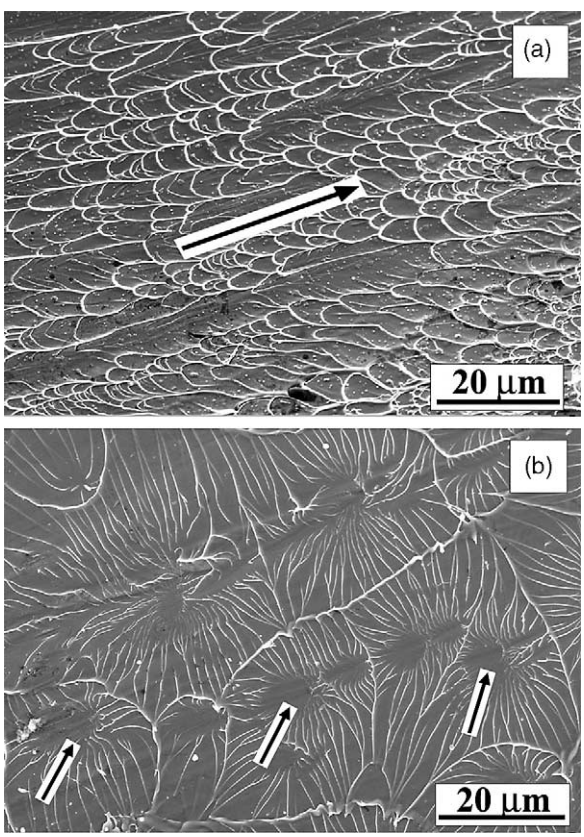


Fig. 5. Comparison of typical fracture features of $Zr_{59}Cu_{20}Al_{10}Ni_8Ti_3$ metallic glassy specimens induced by (a) compressive loading and (b) tensile loading.

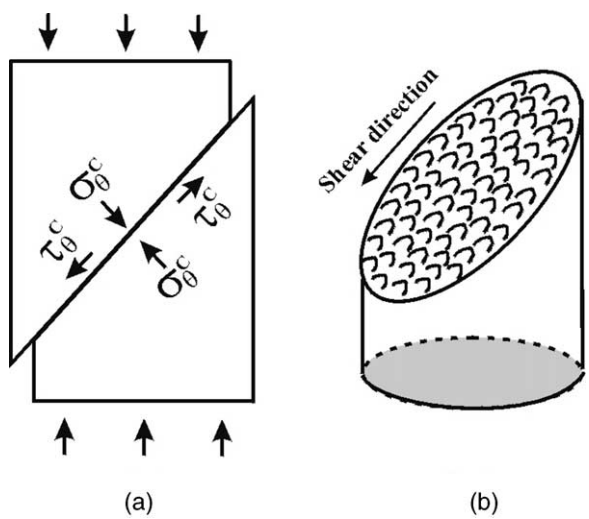


Fig. 6. Illustration of the fracture processes of a metallic glass under compressive deformation. (a) Shear fracture process; (b) vein-like structure.

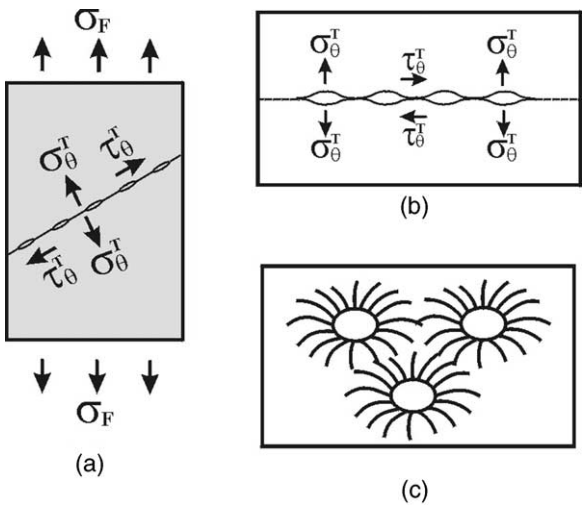


Fig. 7. Illustration of the fracture processes of a metallic glass under tensile deformation. (a) Nucleation of cores; (b) propagation of cores; (c) cores and vein-like structure.

Based on these observations and assumptions, we propose a possible fracture criterion for the metallic glassy specimens under compressive and tensile load, as illustrated in Fig. 8. Since metallic glass is a homogenous material, we may assume that there is critical stress $\tau_0$, as illustrated in Fig. 8(a). $\tau_0$ can be regarded as the critical shear fracture stress on any plane under the condition without normal stress. However, as listed in Tables 1 and 2, the fracture angles ($\theta_C$ and $\theta_T$) always deviate from 45°. This indicates that the normal stress must play an important role in the fracture processes of metallic glasses. Since the fracture stress of metallic glasses is very high (about 1.5–2.0 GPa), the effect of the normal stress applied on the fracture plane should be quite remarkable and can change the critical shear fracture condition of metallic glasses. Donovan [9] and Liu et al. [20] also attributed the deviation of the fracture angle from 45° to the effect of normal stress. In the following, two cases will be considered: (1) when a metallic glass is subjected to a normal compressive stress, $\sigma_C$, on a plane, as illustrated in Fig. 8(b), the critical shear fracture stress, $\tau_C$, on this plane can be expressed as

$$\tau_C = \tau_0 + \mu_C \sigma_C, \tag{1}$$

where $\mu_C$ is a constant for the metallic glass. (2) When a metallic glass is subjected to a normal tension stress, $\sigma_T$, on a plane, as illustrated in Fig. 8(c), the critical shear fracture stress, $\tau_T$, on this plane can be expressed as

$$\tau_T = \tau_0 - \mu_T \sigma_T, \tag{2}$$

where $\mu_T$ is another constant. According to the shear fracture criterion given above, the critical shear fracture conditions for a glassy specimen can be easily obtained. For compressive testing, this yields

$$\tau_\theta^C \geq \tau_0 + \mu_C \sigma_\theta^C, \tag{3}$$

where $\sigma_\theta^C$ and $\tau_\theta^C$ are the normal and shear stresses on the shear plane at compressive fracture, respectively. As illustrated in Fig. 9(a), $\sigma_\theta^C$ and $\tau_\theta^C$ can be calculated from the following equations:

$$\sigma_\theta^C = \sigma_F^C \sin^2(\theta) \tag{4a}$$

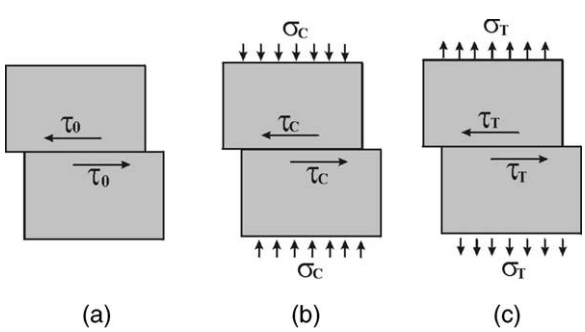


Fig. 8. Illustration of critical fracture stresses of metallic glass. (a) Critical shear fracture stress, $\tau_0$, without normal stress; (b) critical shear fracture stress, $\tau_C$, under the condition with normal compressive stress $\sigma_C$; (c) critical shear fracture stress, $\tau_T$, under the condition with normal tension stress $\sigma_T$.

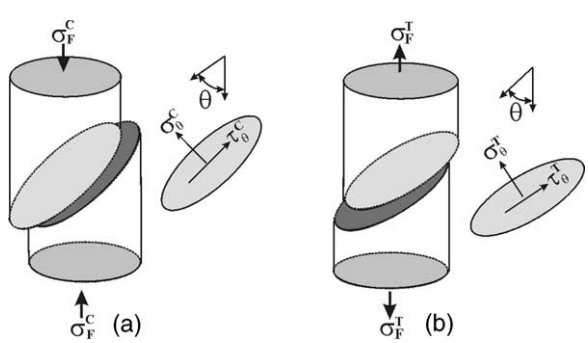


Fig. 9. Illustration of (a) compressive and (b) tensile fracture of the metallic glassy specimen.

$$\tau_\theta^C = \sigma_F^C \sin(\theta)\cos(\theta). \quad (4b)$$

For tensile testing, we can derive

$$\tau_\theta^T \geq \tau_0 - \mu_T \sigma_\theta^T, \quad (5)$$

where $\sigma_\theta^T$ and $\tau_\theta^T$ are the normal and shear stresses on the shear plane at tensile fracture, respectively. As illustrated in Fig. 9(b), they can be expressed as follows:

$$\sigma_\theta^T = \sigma_F^T \sin^2(\theta) \quad (6a)$$

$$\tau_\theta^T = \sigma_F^T \sin(\theta)\cos(\theta) \quad (6b)$$

The variation of $\sigma_\theta^C$ and $\tau_\theta^C$ with the shear angle $\theta$ is illustrated in Fig. 10. By substituting $\sigma_\theta^C$ and $\tau_\theta^C$ into Eq. (3), one gets

$$\sigma_F^C \geq \frac{\tau_0}{\sin(\theta)[\cos(\theta) - \mu_C \sin(\theta)]}. \quad (7)$$

The dependence of $\sigma_\theta^T$ and $\tau_\theta^T$ on the shear angle $\theta$ is also illustrated in Fig. 10. Substituting $\sigma_\theta^T$ and $\tau_\theta^T$ into eq. (5), the critical tensile fracture stress $\sigma_F^T$ can be expressed as

$$\sigma_F^T \geq \frac{\tau_0}{\sin(\theta)[\cos(\theta) + \mu_T \sin(\theta)]}. \quad (8)$$

According to Fig. 10 and Eqs. (7) and (8), it is apparent that the fracture stresses ($\sigma_F^C$ and $\sigma_F^T$) strongly depend on the shear angle $\theta$. There is a minimum value of the two fracture stresses at different shear angle $\theta$. On the other hand, metallic glasses should preferentially fracture along a favorable shear plane at the minimum applied stresses ($\sigma_F^C$ and $\sigma_F^T$). Therefore, the minimum applied fracture stresses ($\sigma_F^C$ and $\sigma_F^T$) must correspond to the measured fracture angles ($\theta_C$ and $\theta_T$), as marked in Fig. 10. Since $\tau_0$ and $\mu_C$ are constants, the critical compressive fracture stress, $\sigma_F^C$, will approach the minimum value at $\theta = \theta_C$ according to the following equation:

$$\frac{\partial(1/\sigma_F^C)}{\partial\theta} = \frac{1}{2\tau_0}[\cos(2\theta_C) - \mu_C \sin(2\theta_C)] = 0. \quad (9)$$

For tensile fracture, the critical tensile fracture stress, $\sigma_F^T$, will also approach the minimum value at $\theta = \theta_T$ according to

$$\frac{\partial(1/\sigma_F^T)}{\partial\theta} = \frac{1}{2\tau_0}[\cos(2\theta_T) + \mu_T \sin(2\theta_T)] = 0. \quad (10)$$

In Eqs. (9) and (10), $\theta_C = 43°$ and $\theta_T = 54°$, therefore, the two constants $\mu_C$ and $\mu_T$ of the present metallic glass can be calculated as follows:

$$\mu_C = \left(\frac{\cos(2\theta_C)}{\sin(2\theta_C)}\right) = \mathrm{ctg}86° = 0.07, \quad (11)$$

$$\mu_T = -\left(\frac{\cos(2\theta_T)}{\sin(2\theta_T)}\right) = -\mathrm{ctg}108° = 0.324. \quad (12)$$

From Eqs. (9) and (10), it can be concluded that the two fracture angles ($\theta_C$ and $\theta_T$) strongly depend on the two constants ( $\mu_C$ and $\mu_T$). In particular, $\mu_C$( = 0.07) is obviously smaller than $\mu_T$( = 0.324), indicating that the normal tension stress $\sigma_\theta^T$ should play a more remarkable role in the fracture process of metallic glass than the normal compressive stress $\sigma_\theta^C$. The deviation of the fracture angle from 45° has been widely observed (see Tables 1 and 2) and can be considered as a natural phenomenon [14–24]. However, the deviation of the tensile fracture angle, $\theta_T$, from 45° is more pronounced than that under compressive fracture, which can be regarded as a direct evidence for the assumptions above. Another evidence is the appearance of the cores on the tensile fracture surfaces, as observed in Figs. 4 and 5. The cores on

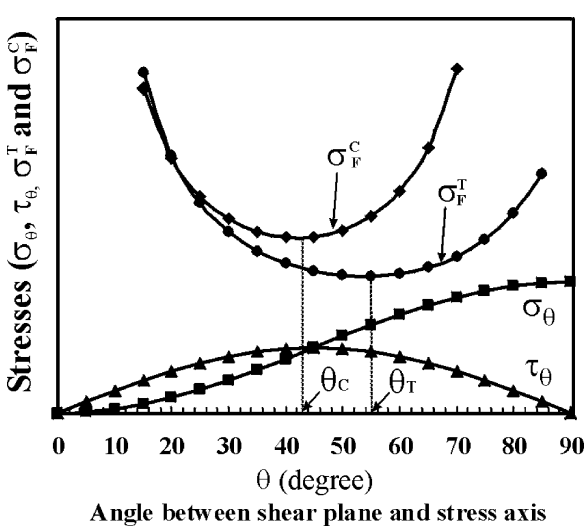


Fig. 10. Illustration of the variation of the normal and shear stresses, fracture stresses on the fracture plane of a specimen under tensile and compressive loading.

the tensile fracture surfaces were never mentioned in detail before and are first discussed in the present work. These cores are believed to be induced by the normal tension stress and can be considered as the origin of tensile fracture. Therefore, the formation of the cores sheds light on the importance of the normal tension stress for the fracture process of metallic glasses.

Meanwhile, from the tensile stress–strain curves of the metallic glass, it is noted that the fracture just occurs at the onset of yielding and there is no plasticity. However, after yielding, the metallic glass can display certain plasticity under compression. The difference in the stress–strain curves between tensile and compressive loading was also widely observed for other metallic glasses [9,16,17,23–28], and will be attributed to the effect of the loading mode or the normal stress too. From the tensile stress–strain curves, it is apparent that yielding, formation of the major shear band, and fracture of the metallic glass occur simultaneously, indicating that the yield stress, $\sigma_Y^T$, corresponds to the fracture stress, $\sigma_F^T$, under tensile deformation. However, under compression, the deformation and fracture processes can be divided into three stages: (1) yielding and formation of shear bands; (2) propagation of formed shear bands and formation of new shear bands; this stage corresponds to the plastic deformation of metallic glass; (3) local cracking along the shear bands and final fracture along the major shear band. From the stress–strain curves in Fig. 2(a), it is known that the compressive yield stress $\sigma_Y^C$( = 1.45 GPa) is slightly lower than the compressive fracture stress $\sigma_F^C$( = 1.69 GPa). This means that there may be some strain hardening during the plastic deformation of the metallic glass under compression. This strain hardening process should correspond to the propagation of shear bands and the formation of new shear bands, as shown in Fig. 3(f).

If the fracture angles, $\theta_C$ and $\theta_T$, under the two different loading modes are considered, the yield shear stresses $\tau_Y^C$ and $\tau_Y^T$ on the compressive and tensile fracture planes of the metallic glass can be calculated from the following equations:

$$\tau_Y^C = \sigma_Y^C \sin(\theta_C)\cos(\theta_C) = 0.73 \text{ (GPa)}, \quad (13)$$

$$\tau_Y^T = \sigma_Y^T \sin(\theta_T)\cos(\theta_T) = 0.75 \text{ (GPa)}. \quad (14)$$

The results above indicate that the yield shear stresses $\tau_Y^C$ and $\tau_Y^T$ on the fracture plane of metallic glass are nearly the same even though the normal yield stresses ($\sigma_Y^C$ and $\sigma_Y^T$) have a large difference for the two loading modes. This, in turn, demonstrates that the critical yield shear stresses of metallic glass are identical under compression and tension. However, due to the difference in the deformation modes, the normal tension stress will promote the fracture of metallic glass, which results in the simultaneous occurrence of yield and tensile fracture. In contrast, the normal compressive stress can restrain the activation of shear bands and the fracture of the metallic glass, as a result, occurs by the propagation of shear bands and the formation of new shear bands [30]. This process, in turn, increases the stress necessary for activating shear bands and the fracture stress of the metallic glass. Therefore, it can be concluded that the difference in the deformation and fracture processes of metallic glasses can be mainly attributed to the difference in the loading modes.

Furthermore, under tensile loading, it is noted that the normal stress, $\sigma_\theta^T$, increases rapidly with increasing shear angle $\theta$, as illustrated in Fig. 10, whereas the shear stress, $\tau_\theta^T$, decreases slowly for $\theta \geq 45°$. This gives a critical tensile fracture condition for a fracture angle larger than 45° when taking both normal and shear stresses into account. This explains why metallic glasses do not fracture along the maximum shear plane, but along a shear angle larger than 45°. From the proposed fracture criterion, the fracture of metallic glasses often occurs along a favorable shear angle $\theta_T \geq 45°$, which results in the decrease in the fracture stresses $\sigma_F^T$ than that along the maximum shear stress plane. This indicates that the normal tension stress, $\sigma_\theta^T$, can promote the shear fracture of metallic glasses, and the larger tensile fracture angle, $\theta_T$, corresponds to a higher normal tension stress, $\sigma_\theta^T$, on the fracture plane. Therefore, the large deviation of the fracture angle, $\theta_T$, from 45° can be understood. However, under compressive loading, the fracture process is mainly controlled by the shear stress on the fracture plane. A smaller $\theta_C$ will reduce the shear stress on the fracture plane, which explains why the compressive fracture angle, $\theta_C$, does not show a significant deviation from 45°.

Following the fracture criterion given above, the effect of different deformation modes and the applied stress on the fracture processes of metallic glasses can be illustrated as in Fig. 11(a). In this figure, the critical shear fracture stress, $\tau_0$, is regarded identical since the two specimens have the same composition. For the metallic glassy specimen subjected to a tensile load, with increasing tensile stress $\sigma_T$, the resolved shear stress $\tau_\theta^T( = \theta_T \sin(\theta_T) \cos(\theta_T))$ applied on the fracture plane increases along line 1. In contrast, the critical shear fracture stress $\tau_T( = \tau_0 - \mu_T\sigma_\theta^T)$ will drop along line 2 according to Eq. (5). When the two stresses ($\tau_\theta^T$ and $\tau_T$) reach the same value, the applied tensile stress corresponds to the tensile fracture strength $\sigma_F^T$, as marked in the figure. For a metallic glassy specimen subjected to a compressive load, with increasing compressive stress, $\sigma_C$, the resolved shear stress $\tau_\theta^C( = \sigma_C \sin(\theta_C) \cos(\theta_C))$ applied on the fracture plane should increase along line 3. The critical shear fracture stress $\tau_C( = \tau_0 + \mu_C\sigma_\theta^C)$ also increases slowly along line 4. In this case, the two stresses ($\tau_\theta^C$ and $\tau_C$) will meet at the compressive fracture strength $\sigma_F^C$, as marked in the figure. Therefore, the stress state and the fracture processes of metallic glass are quite different for the different deformation modes.

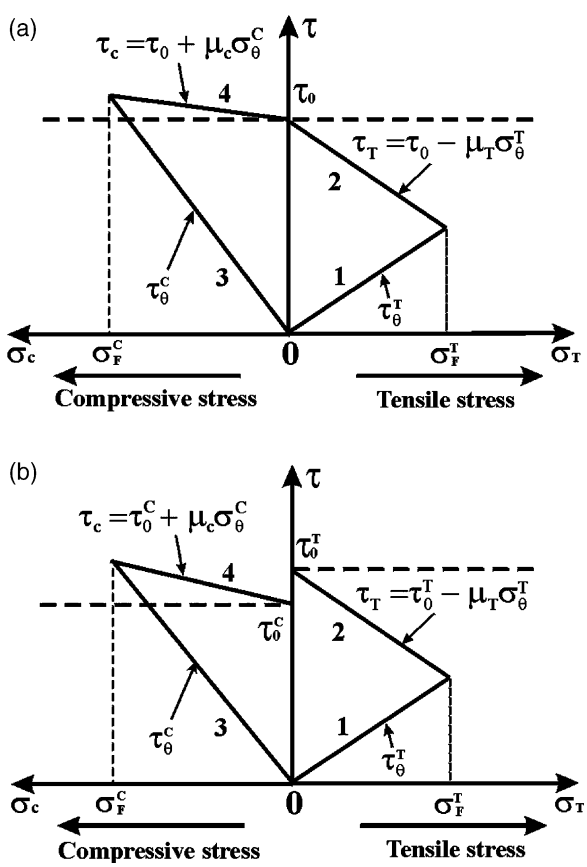


Fig. 11. Variation of the compressive $\sigma_F^C$ and tensile fracture stress $\sigma_F^T$, normal stress, $\sigma_\theta$, and shear stresses, $\tau_\theta$, on the fracture angle $\theta$ under tensile and compressive loading.

If $\tau_0^C$ and $\tau_0^T$ represent the critical shear fracture stresses of the compressive and tensile specimens, they can be calculated using Eqs. (7) and (8). Since the fracture stresses $\sigma_F^C( = 1.69$ GPa) and $\sigma_F^T$ (1.58 GPa) in Eqs. (7) and (8) are known, substituting $\theta = \theta_T = 54°$ and $\theta = \theta_C = 43°$, one gets

$$\tau_0^C = \sigma_F^C \sin(\theta_C)[\cos(\theta_C) + \mu_C \sin(\theta_C)] \quad (15)$$

$$= 0.8 \text{ (GPa)},$$

$$\tau_0^T = \sigma_F^T \sin(\theta_T)[\cos(\theta_T) + \mu_T \sin(\theta_T)] \quad (16)$$

$$= 1.1 \text{ (GPa)}.$$

From the above results, we find that the critical shear fracture stress $\tau_0^T$ (1.1 GPa) of the tensile specimen is slightly higher than the critical stress $\tau_0^C$ (0.8 GPa) of the compressive specimen. Since the compositions of the two metallic glasses are identical, the critical shear fracture stresses, $\tau_0^C$ and $\tau_0^T$ should also be the same. However, as shown in Fig. 1, it can be seen that the XRD patterns of the metallic glass rod and plate are somewhat different. This might reflect some difference in the structures of the two metallic glasses because the cooling conditions of the two kinds of specimens are somewhat different during casting. Besides, the shapes of the two kinds of specimens are also different, i.e. 3 mm in diameter for compressive specimens and 6 mm × 3 mm × 1.5 mm for tensile specimens. Therefore, the difference in the structure and shape of the compressive and tensile specimens might affect the critical shear fracture stresses $\tau_0^C$ and $\tau_0^T$ of the metallic glass and the calculated results from Eqs. (15) and (16) are also acceptable. In this case, for the two kinds of specimens, the effect of the applied stresses on the fracture processes can be illustrated as in Fig. 11(b). The critical shear fracture stress, $\tau_0^C$ of the compressive

specimen is smaller than the critical shear fracture stresses, $\tau_0^T$ of the tensile specimen. However, this change should not affect the general understanding of the fracture criterions of metallic glasses under compressive and tensile loading.

## 5. Conclusions

1. As in most metallic glasses, $Zr_{59}Cu_{20}Al_{10}Ni_8Ti_3$ BMG displays a different deformation and fracture behavior under compressive and tensile loading. Under compression, the metallic glass displays some plasticity before fracture. The fracture angle, $\theta_C$, between the stress axis and the fracture plane is 43°. Under tensile loading, however, the metallic glass always displays brittle fracture without yielding. The tensile fracture angle $\theta_T$( = 54°) between the stress axis and the fracture plane is obviously larger than 45°. Therefore, both $\theta_C$ and $\theta_T$ deviate from the maximum shear stress plane (45°), indicating that the fracture behavior of the metallic glass under compressive and tensile load does not follow the von Mises criterion.
2. Fracture surface observations reveal the difference in the fracture mechanisms induced compressive and tensile load. Under compression, the fracture surface only consists of a quite uniform vein-like structure. However, a combined fracture feature of veins and some cores is observed on the tensile fracture surfaces. The difference in the fracture mechanisms of the metallic glass is attributed to the effect of the normal stress on the fracture process. It is considered that the radiating cores on the fracture surface are produced by the normal tension stress in the initial stage of fracture, the veins are mainly created by the shear stress during rapid shear propagation. However, the compressive fracture of metallic glass should be mainly controlled by the shear stress. Due to the different effect of the normal stress on the fracture processes under compressive and tensile load, the deviation of $\theta_C$ and $\theta_T$ from 45° shows a large difference.

## Acknowledgements

The authors would like to thank H. Grahl, H. Schulze, R.-H. Reiter and A. Schwab for sample preparation and H.-J. Klauß for assistance with the mechanical tests, and G. He, A. Güth for stimulating discussions. This work was supported by the German Science Foundation (DFG) under grant EC 111/10-1 and by the EU via the RTN-Network on bulk metallic glasses under contract HPRN-CT-2000-00033. One of the authors (Z.F. Zhang) wishes to acknowledge the Alexander von Humboldt (AvH) Foundation for providing a postdoctoral fellowship.

## References

[1] Johnson WL. MRS Bull 1999;24(10):42.
[2] Inoue A. Acta Mater 2000;48:279.
[3] Pampillo CA. Scripta Metall 1972;6:915.
[4] Leamy HJ, Chen HS, Wang TT. Metall Trans A 1972;3:699.
[5] Pampillo CA. J Mater Sci 1975;10:1194.
[6] Spaepen F. Acta Metall 1977;25:407.
[7] Argon AS. Acta Metall 1979;27:47.
[8] Steif PS, Spaepen F, Hutchinson JW. Acta Metall 1982;30:447.
[9] Donovan PE. Acta Mater 1989;37:445.
[10] Leng Y, Courtney TH. J Mater Sci 1991;26:588.
[11] Chen H, He Y, Shiflet GJ, Poon SJ. Nature 1994;367:541.
[12] Huang R, Suo Z, Prevost JH, Nix WD. J Mech Phys Solid 2002;50:1011.
[13] Honeycombe RWK. Plastic deformation of metals. Cambridge: Cambridge University Press, 1969.
[14] Donovan PE. Mater Sci Eng 1988;98:487.
[15] Lowhaphandu P, Montgomery SL, Lewandowski JJ. Scripta Mater 1999;41:19.
[16] Wright WJ, Saha R, Nix WD. Mater Trans JIM 2001;42:642.
[17] He G, Lu J, Bian Z, Chen DJ, Chen GL, Tu GH et al. Mater Trans JIM 2001;42:356.
[18] Takayama S. Scripta Metall 1979;13:463.
[19] Megusar J, Argon AS, Grant NJ. Mater Sci Eng 1979;38:63.
[20] Liu CT, Heatherly L, Easton DS, Carmichael CA, Schneibel JH, Chen CH et al. Metall Mater Trans A 1998;29:1811.
[21] Fan C, Inoue A. Mater Trans JIM 1999;40:1376.
[22] Inoue A, Kimura HM, Zhang T. Mater Sci Eng A 2000;294–296:727.
[23] Inoue A, Zhang W, Zhang T, Kurosaka K. Acta Mater 2001;49:2645.

[24] Mukai T, Nieh TG, Kawamura Y, Inoue A, Higashi K. Scripta Mater 2002;46:43.
[25] Leohard A, Xing LQ, Heilmaier M, Gebert A, Eckert J, Schultz L. Nanostruct Mater 1998;10:805.
[26] Heilmaier M. J Mater Proc Tech 2001;117:374.
[27] Subhash G, Dowing RJ, Kecskes LJ. Mater Sci Eng A 2002;334:33.
[28] Zhang T, Inoue A. Mater Trans JIM 1998;39:1230.
[29] Zhang T, Inoue A. Mater Sci Eng 2001;304–306:771.
[30] Hufnagel TC, El-Deiry P, Vinci RP. Scripta Mater 2000;43:1071.